A report to the sponsors of the
Exploration Geophysics Laboratory

# 2-D Modeling of Direct-S and Direct-P Wavefields

## Part 1: Modeling Principles and Examples

Bob Hardage and Don Wagner

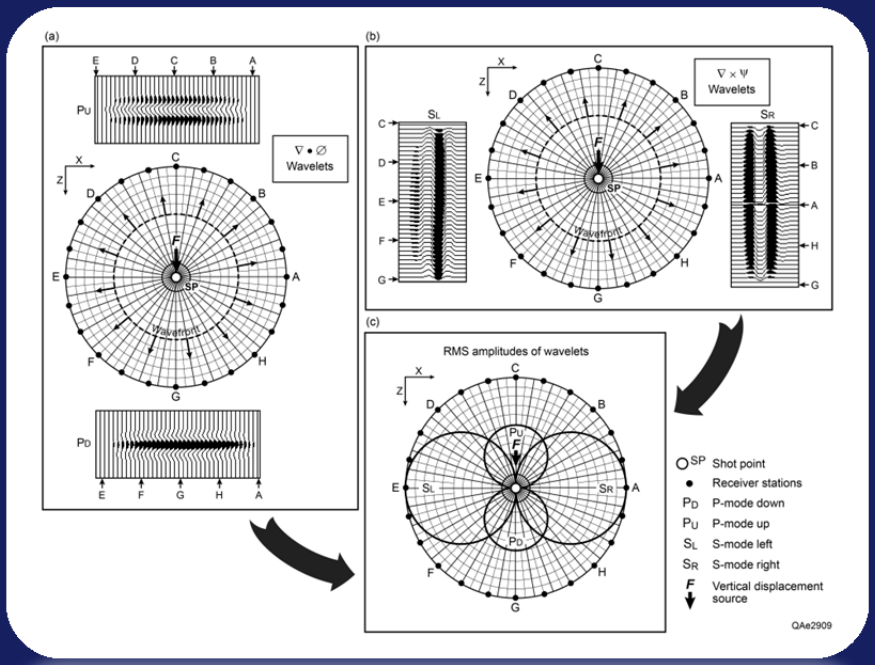


September 2014

EGL Exploration Geophysics Laboratory

Bureau of Economic Geology

QAe2977

# 2-D Modeling of Direct-S and Direct-P Wavefields
# Part 1: Modeling Principles and Examples

**Bob Hardage and Don Wagner**
**September 2014**

## Introduction

The Exploration Geophysics Laboratory (EGL) has implemented a 2-D finite-difference modeling algorithm that simulates direct-P and direct-S propagation in a user-defined earth medium. The output of this modeling code illustrates direct-mode and converted-mode reflections, provides information that aids in positioning receivers around source stations so there is optimal illumination of geologic targets, assists data processors by showing relative-amplitude behaviors of key reflections, and shows interferences between S-mode and P-mode reflection events. EGL is finding this modeling code to be a great asset for ensuring direct-S modes produced by vertical-displacement sources are properly recorded and processed. This report is the first of a series of sponsor reports based on model-generated data. The purpose of these reports is to illustrate wavefield propagation physics of direct-P and direct-S modes produced by vertical-displacement and horizontal-displacement sources. These reports should lead to improved understanding of direct-S reflectivity and assist in developing data-processing procedures for extracting direct-S information from vertical-displacement-source data. This initial report summarizes the principles of the modeling code.

Similar codes have been discussed in the literature for three decades or longer (e.g. Wapenaar et al., 1990), and equivalent modeling capabilities exist inside numerous organizations. If modeling capability like that described in this report is not available to an EGL sponsor, EGL can do a reasonable amount of modeling effort for a sponsor who wishes to investigate and apply direct-S technology

## Overview of Modeling Code Capabilities

The EGL modeling code described in this report is applied to a user-defined, 2-D, layered-earth model in which $V_P$, $V_S$, $\rho$, $Q_P$, $Q_S$, Thomsen parameters, and anisotropic stiffness coefficients are assigned to earth layers in seismic-wave propagation space ($V_P$ = P-wave velocity; $V_S$ = S-wave velocity; $\rho$ = bulk density; $Q_P$ = P-wave damping factor; $Q_S$ = S-wave damping factor). EGL uses log data to define these earth-layer parameters whenever possible. There is no limit to the number of earth layers that can be used in a calculation other than the practicality of avoiding excessive compute time. The code allows earth layers to have lateral variations in physical properties, thus structure, pinchouts, facies distributions, and stratigraphic anomalies can be included in a 2-D model. Model output shown in this Part-1 report will be 2-dimensional profiles in planes passing through a single source station and a selected distribution of receiver stations. In this initial report, layer interfaces will be flat and horizontal, and layers will consist of only homogeneous rocks.

The earth displacement that a model source creates can be vertical or horizontal. There are no software restrictions on source station spacing or on the number of source stations in a profile. Receivers can be either vertical geophones or horizontal geophones. Receivers can be distributed in 2-D model space to simulate a surface receiver array, a vertical sensor array, a circle of receivers around a source station, or any arbitrary 2-D arrangement of receivers. The separation between adjacent receiver stations can be any desired distance.

(a) *Lamé's Theorem*

(1) $u = \nabla\phi + \nabla\times\psi$

u = Displacement field
$\phi$ = P-wave potential
$\psi$ = S-wave potential
$\nabla\phi$ = P-wave component of u
$\nabla\times\psi$ = S-wave component of u

(b) *Far-field P-wave*

(2) $u_i^P(x, t) = \frac{1}{4\pi\rho\alpha^2}\gamma_i\gamma_j\frac{1}{r}X_0\left(t - \frac{r}{\alpha}\right)$

(c) *Far-field S-wave*

(3) $u_i^S(x, t) = \frac{1}{4\pi\rho\beta^2}(\delta ij - \gamma_i\gamma_j)\frac{1}{r}X_0\left(t - \frac{r}{\beta}\right)$

$\gamma_j X_0$ = Point source acting in direction j
$u_i^P$ = Displacement parallel to direction from source
$u_i^S$ = Displacement normal to direction from source
$\gamma$ = Direction cosine
$\delta$ = Kronecker delta

$\alpha$ = P-wave velocity $\beta$ = S-wave velocity $\rho$ = Density

QAe2699

Figure 1. Mathematical basis of modeling code.

The code is a finite-difference solution of the wave equations that define 2-D propagation of direct-P and direct-S modes produced by a seismic source. The number of earth layers and receiver stations should always be large numbers so the finite-difference grid across the earth model is finely sampled in both the vertical and horizontal dimensions of model space. The representation and propagation of direct-P and direct-S wavefields from a source station are described by Lame's theorem defined in Figure 1a. The divergence and curl operations (Eq. 1, Fig. 1a) that generate the P-wave and S-wave components of a propagating displacement wavefield **u** are calculated in spherical coordinates, resulting in a **(1/r)** (r = propagation distance) amplitude decay factor in P and S displacements (Eq. 2, Fig. 1b and Eq. 3, Fig. 1c). Relative amplitudes between P and S reflections from a targeted interface in the 2-D models that are created are thus realistic representations of relative amplitudes of P and S reflections embedded in real seismic data.

Equation 2 (Fig. 1b) describes P-wave displacement produced by wavefield propagation resulting from a specific source displacement applied in a defined 2-D model space. Equation 3 (Fig. 1c) describes S-wave displacement produced by the same 2-D propagating wavefield.

These equations describe the modes that are initiated at the source station. After initiation, each wave type converts to other modes where an illuminating wavefield encounters an impedance contrast (e.g. P converts to SV, and SV converts to P).

## Modeling Examples

### Section Views of Direct-P and Direct-S Radiation Patterns

It is essential to understand the P and S radiation patterns produced by the modeling code, thus a simple earth model was created to illustrate the geometry of direct-P and direct-S radiations that propagate away from a source station occupied by either a vertical-displacement source or a horizontal-displacement source. This hypothetical earth model is illustrated in Figure 2 and is based on the following assumptions:

1. The earth is a constant-velocity, homogeneous medium in which $V_P$ = 10,000 ft/s and $V_S$ = 5,000 ft/s throughout the entire model space.
2. The source is embedded in the interior of this hypothetical earth at spatial coordinates (X, Z) = (10,000 ft, 10,000 ft), where X is horizontal distance and Z is depth.
3. Radial and transverse geophones are distributed in a circle surrounding the buried source station. The radius of the receiver circle is 2000 ft.

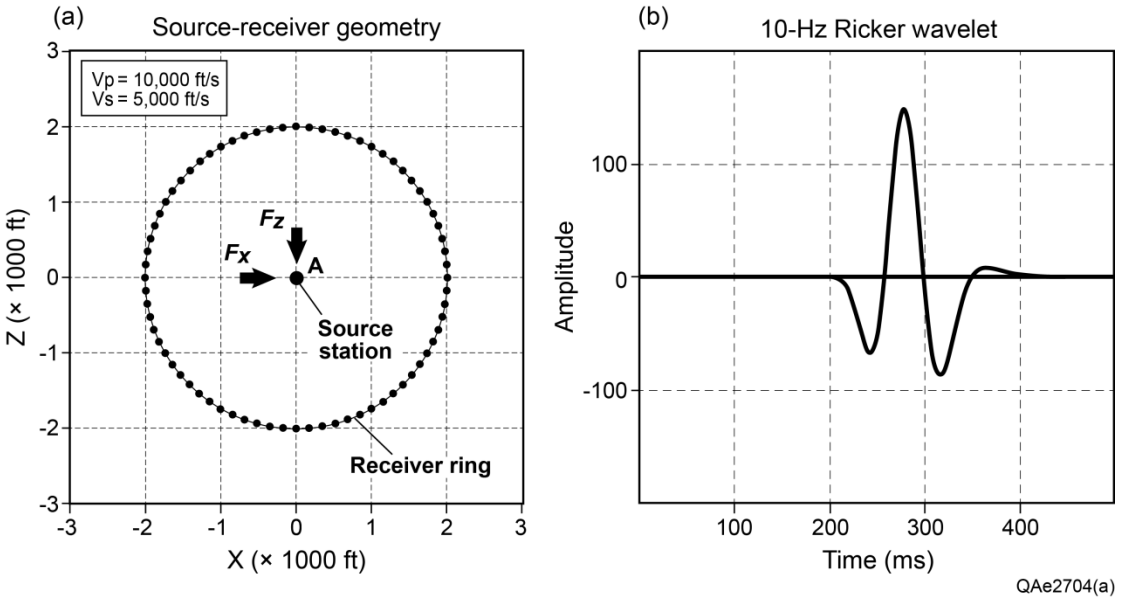


Figure 2. (a) Earth model and source-receiver geometry used to analyze direct-P and direct-S radiation patterns produced by a vertical-displacement source and a horizontal-displacement source. Each receiver station, shown as a solid dot on the receiver ring, is occupied by a vertical geophone and a horizontal geophone. Wavefields produced by both vertical-displacement sources ($F_Z$) and horizontal-displacement sources ($F_X$) will be studied. (b) The source wavelet that propagates in the earth medium.

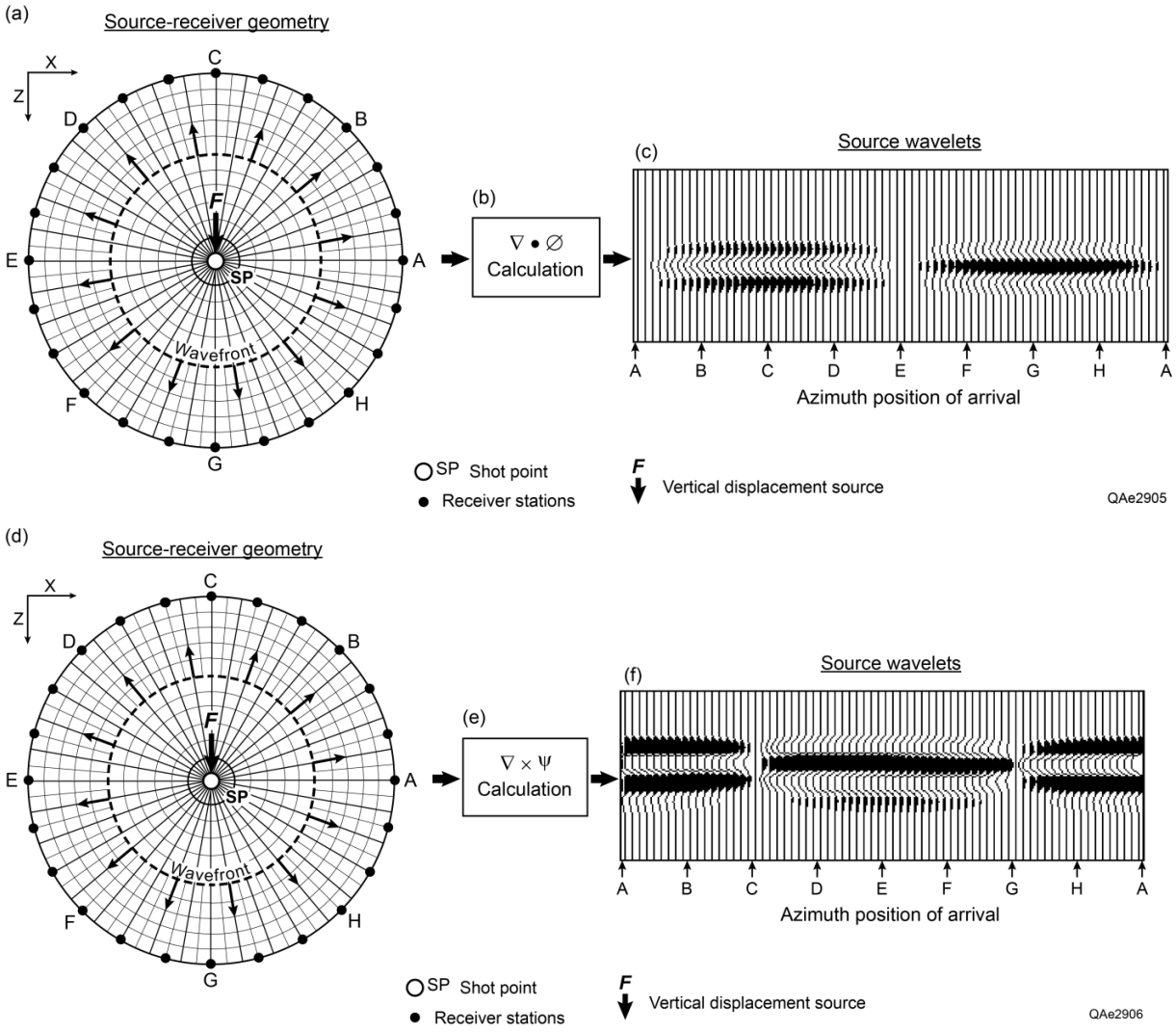


Figure 3. Direct-P and direct-S wavefields produced by a vertical-displacement source. (a) Source-receiver geometry. (b) Calculation of P-wave component of wavefield. (c) P wavelets that arrive at receiver stations. (d) Repeat of source-receiver geometry. (e) Calculation of S-wave component of wavefield. (f) S wavelets that arrive at receiver stations. The orientations of the horizontal geophone (X) and the vertical geophone (Z) at each source station are shown by the X-Z coordinate system in (a) and (d). The radial arrows on the dashed wavefronts in (a) and (d) indicate the directions that raypaths expand away from the source station. The P-wave displacements in (c) are in the same direction as these raypaths. The S displacements in (f) are perpendicular to the same raypaths.

The direct-P and direct-S radiated wavelets generated in this model medium by a vertical-displacement source are shown in Figure 3, and wavelets produced by a horizontal-displacement source are shown in Figure 4. The vertical-force displacement wavefield that propagates away from the source is illustrated in Figures 3a and 3d as an expanding circle mid-way between the source station and the ring of receiver stations. The calculation of the P-wave component of the wavefield is illustrated in Figures 3b and 3c, and the construction of

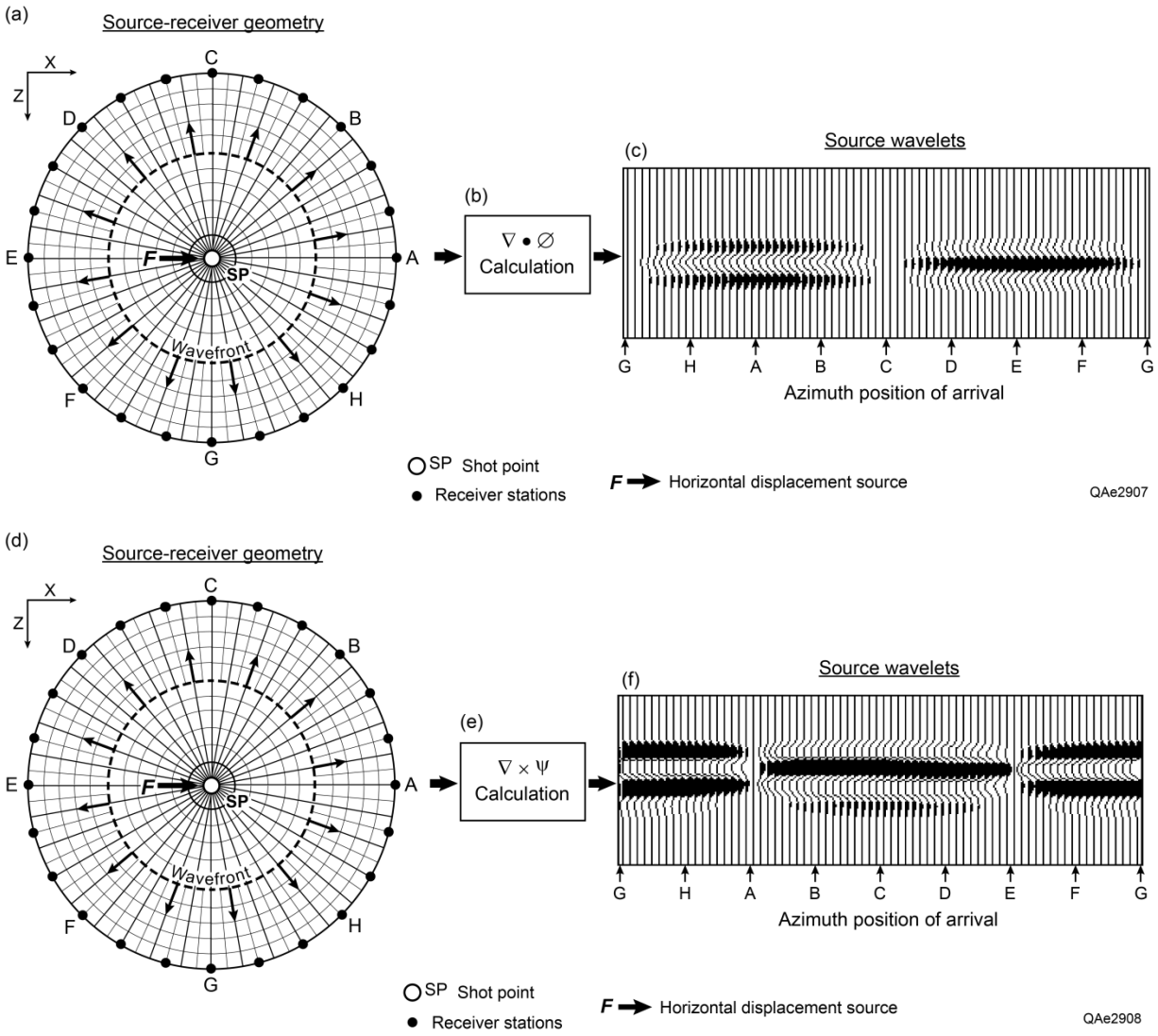


Figure 4. Direct-P and direct-S wavefields produced by a horizontal-displacement source. (a) Source-receiver geometry. (b) Calculation of P-wave component of wavefield. (c) P wavelets that arrive at receiver stations. (d) Repeat of source-receiver geometry. (e) Calculation of S-wave component of wavefield. (f) S wavelets that arrive at receiver stations. Orientations of the horizontal geophone (X) and the vertical geophone (Z) at each source station are shown by the X-Z coordinate system added to panels (a) and (d). The radial arrows on the dashed wavefronts in (a) and (d) indicate the directions that raypaths expand away from the source station. The P-wave displacements in (c) are in the same direction as these raypaths. The S displacements in (f) are perpendicular to the raypaths.

the S-wave component of the displacement wavefield is shown as Figures 3e and 3f.
The azimuth distributions of the direct-P and direct-S arrivals at the circular receiver array surrounding the source station is indicated by receiver station labels (A, B, C, . . .) added to the wavelets in Figures 3c and 3f. This same graphics format is used in Figure 4 to show the direct-P and direct-S displacements that are generated by a horizontal-displacement source positioned

at the same source station. Note the differences between the azimuth distributions of direct-P wavelets in Figure 4c and direct-S wavelets in Figure 4f compared to the azimuth distributions of P and S wavelets generated by the vertical-displacement source in Figures 3c and 3f.

The P and S wavelets that arrive at the receiver stations surrounding shot point SP are shown in their relative amplitude forms in Figures 3c, 3f and 4c, 4f. The RMS values of these relative amplitudes are good measures of the strengths of P and S radiation in all possible take-off angles from the source station. The conversion of these first-arrival wavelets into radiation-strength lobes is illustrated in Figure 5 for a vertical-displacement source and in Figure 6 for a horizontal-displacement source.

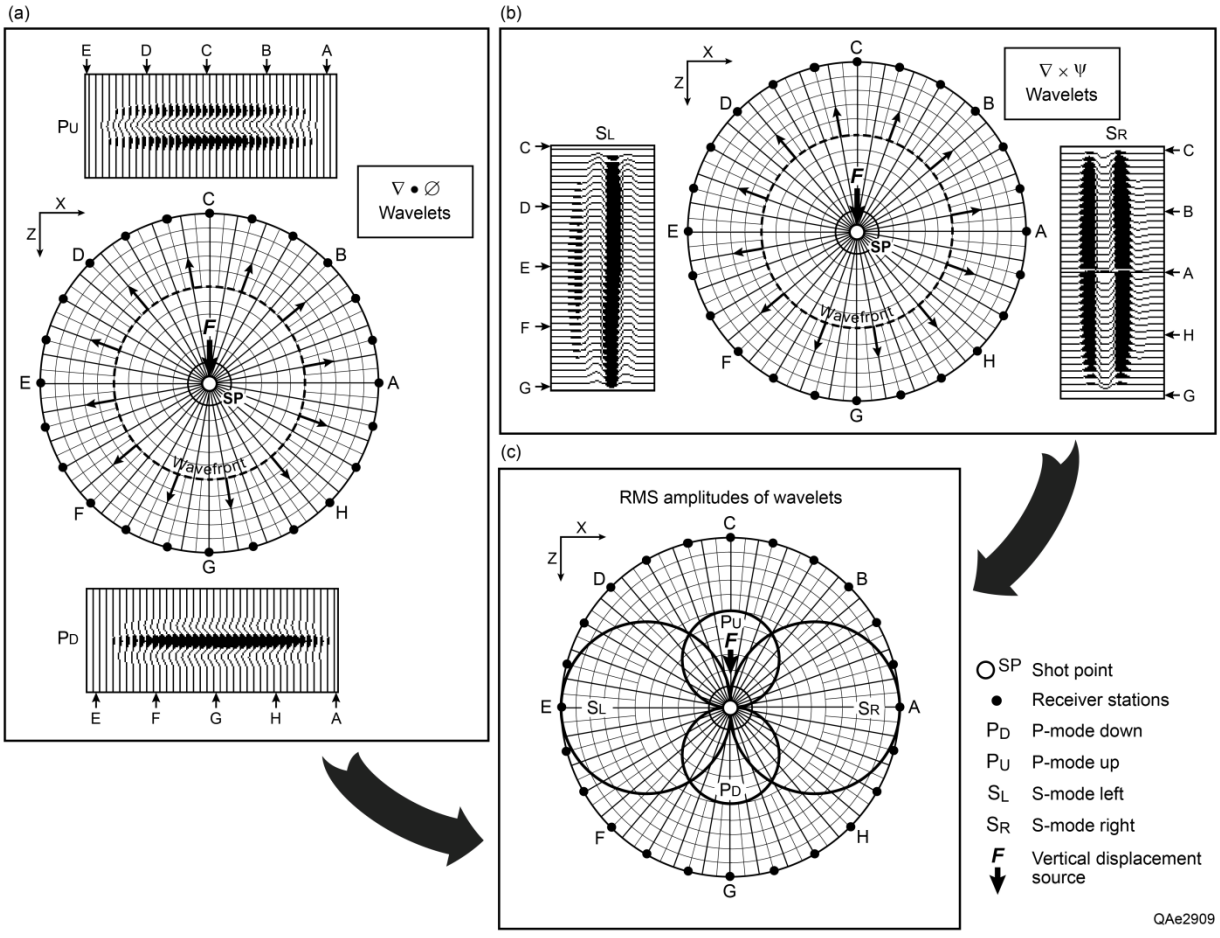


Figure 5. Construction of P and S radiation patterns created by a vertical-displacement source. (a) Distribution of P-wavelets produced at shot point SP and recorded by the surrounding circular array of receiver stations (Fig. 2). (b) Distribution of S-wavelets produced at shot point SP and recorded at surrounding receiver stations. (c) RMS amplitudes of these P and S wavelets at all possible take-off angles from source station SP. Orientations of the horizontal geophone (X) and vertical geophone (Z) at each source station are shown by the X-Z coordinate system in each panel.

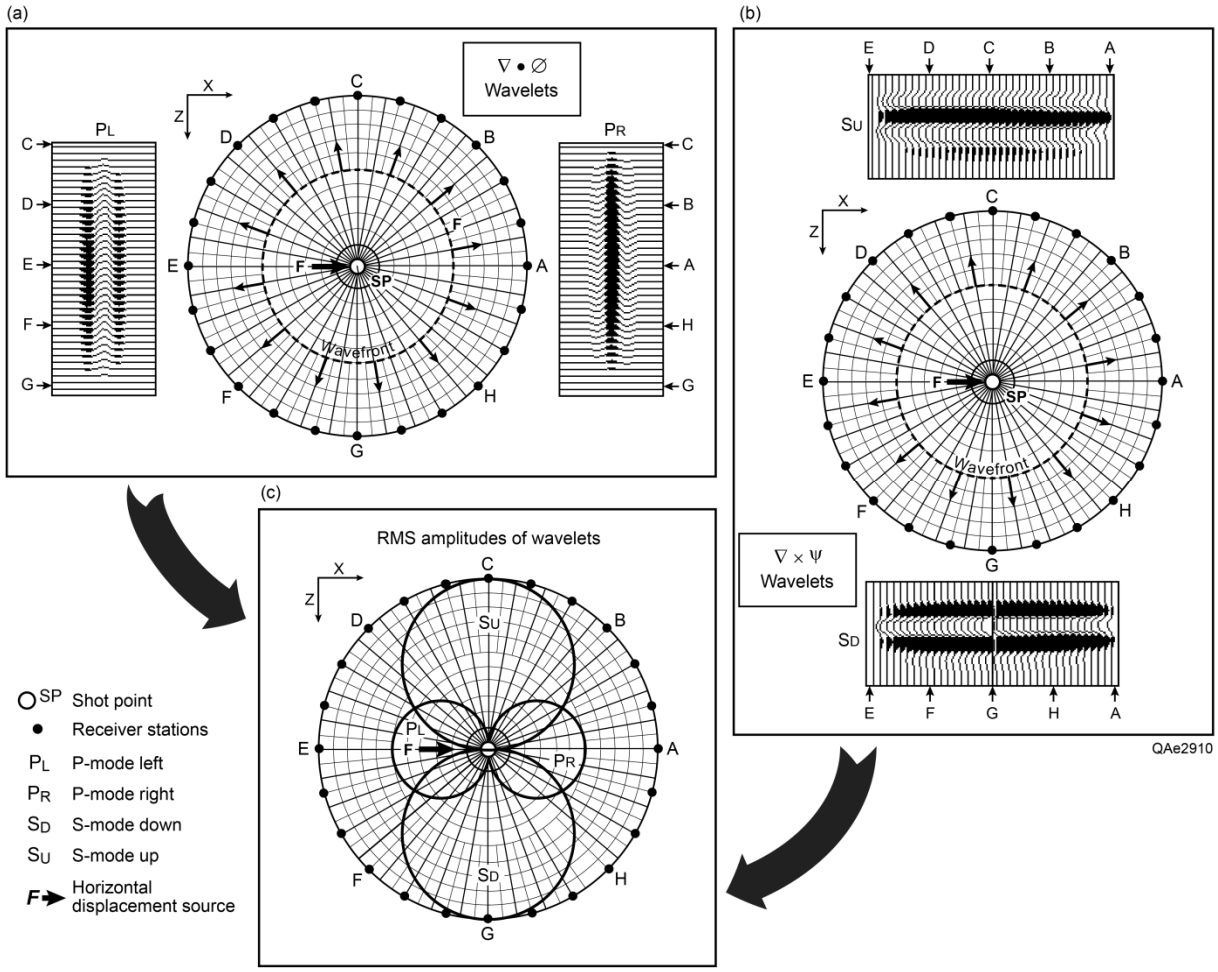


Figure 6. Construction of P and S radiation patterns for a horizontal-displacement source.
(a) Distribution of P-wavelets produced at shot point SP and recorded at surrounding receiver stations.
(b) Distribution of S-wavelets produced at shot point SP and recorded at surrounding receiver stations.
(c) RMS amplitudes of these P and S wavelets at all possible take-off angles from source station SP.
Orientations of the horizontal geophone (X) and vertical geophone (Z) at each source station are shown by the X-Z coordinate system in each panel.

The radiation patterns in Figures 5 and 6 emphasize several principles observed in real seismic field data: (a) both horizontal-displacement and vertical-displacement sources create direct-P and direct-S modes, (b) direct-S amplitudes are much stronger than direct-P amplitudes, and (c) direct-S and direct-P modes produced by a vertical-displacement source radiate energy at take-off angles that differ by $90^{o}$ from the take-off angles associated with direct-S and direct-P modes produced by a horizontal-displacement source. Regarding principle (b), the sizes of the radiation patterns in Figures 5 and 6 are drawn arbitrarily for graphical simplicity and for easier labeling of features related to the radiation patterns. The actual P and S radiation patterns that result from this modeling exercise are shown in Figure 7 in their correct relative sizes. In this hypothetical propagation medium (Fig. 7a), the S radiation strength is approximately seven times stronger than the P radiation strength.

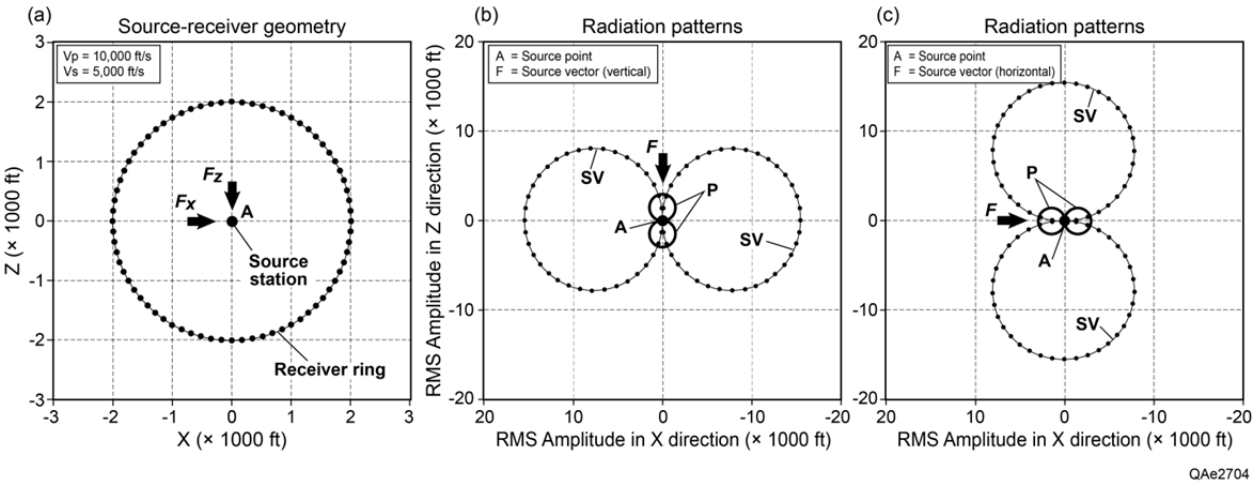


Figure 7. P and S radiation patterns produced by the earth model shown in Figure 2. (a) Repeat of earth model. (b) P and S patterns produced by vertical-displacement source $F_Z$. (c) P and S patterns produced by horizontal-displacement source $F_X$. For either source, S radiation is larger than P radiation by a factor of 7X. These diagrams show only the amplitudes of the P and S wavelets traveling in each take-off angle direction from a source. The patterns do not define the polarities of those propagating wavelet, nor do they indicate propagation velocities.

The model in Figure 2a (and in Figure 7a) allows no interface to be local to the source station. Thus the claim by some that S-wave modes that propagate away from a vertical-displacement source station cannot be direct-S modes, but have to be converted-S modes generated by P-to-SV mode conversions at an interface local to a source station, is invalid. Sources were deliberately not positioned on an earth-air interface as a source would be in real-world seismic data acquisition. By avoiding the existence of any near-source earth layer, the point of origin of direct-S modes is clearly defined.

An additional property of direct P and S radiation patterns that needs to be illustrated is the polarities of the P and S displacements associated with expanding P and S radiation lobes. To determine P and S radiation polarity, the orientations of X and Z receivers need to be compared with the polarities of the displacement vectors associated with wavefront expansion in take-off angles that differ by 180 degrees. If receiver orientation and wavefront displacement direction are the same at a receiver station, wavelet polarity is positive. If receiver orientation and wavefront displacement direction are opposite, wavelet polarity is negative. Examination of Figure 5a shows that above horizontal line AE, the vertical components of wavefront displacements are opposite to the orientations of vertical geophones (Z). Thus upgoing P wavelets have negative polarity. Below line AE, the vertical components of wavefront displacements are aligned with the Z geophones, which create positive-polarity downgoing wavelets. This wave physics means that the polarity of recorded P wavelets in upgoing lobe $P_U$ is opposite to the polarity of recorded P wavelets in downgoing lobe $P_D$ (Fig. 5c).

Comparing orientations of horizontal components of wavefield displacements with the orientations of X geophones on the right and left of vertical line CG (Fig. 5b) leads to a similar

conclusion – the polarity of recorded S wavelets in right-going lobe $S_R$ is opposite to the polarity of recorded S wavelets in left-going lobe $S_L$ (Fig. 5c). Thus the polarities of all four radiation lobes created by a vertical-displacement source are as shown by the wave-mode displacement vectors in Figure 8. A similar analysis of Figure 6 leads to the conclusion that the polarities of all four radiation lobes generated by a horizontal-displacement source are as shown in Figure 9.

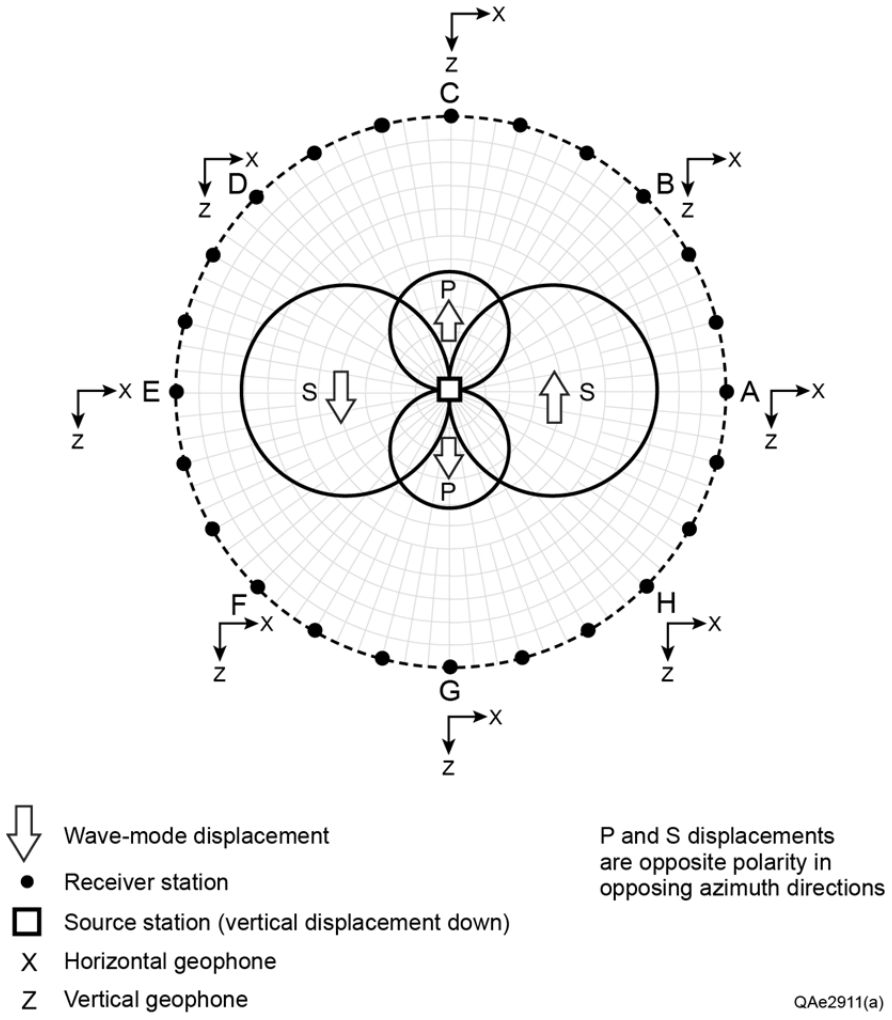


Figure 8. Polarities of recorded P and S displacements created by a vertical-displacement source when the surrounding X and Z receivers are deployed as shown.

## Section Views of Direct-P and Direct-S Propagating Wavefronts

The earth models in Figure 3a,d and 4a,d are now used to illustrate the propagation of direct-P and direct-S wavefronts away from a buried source station. The positions of propagating direct-P and direct-S wavefronts produced by a vertical-displacement source are

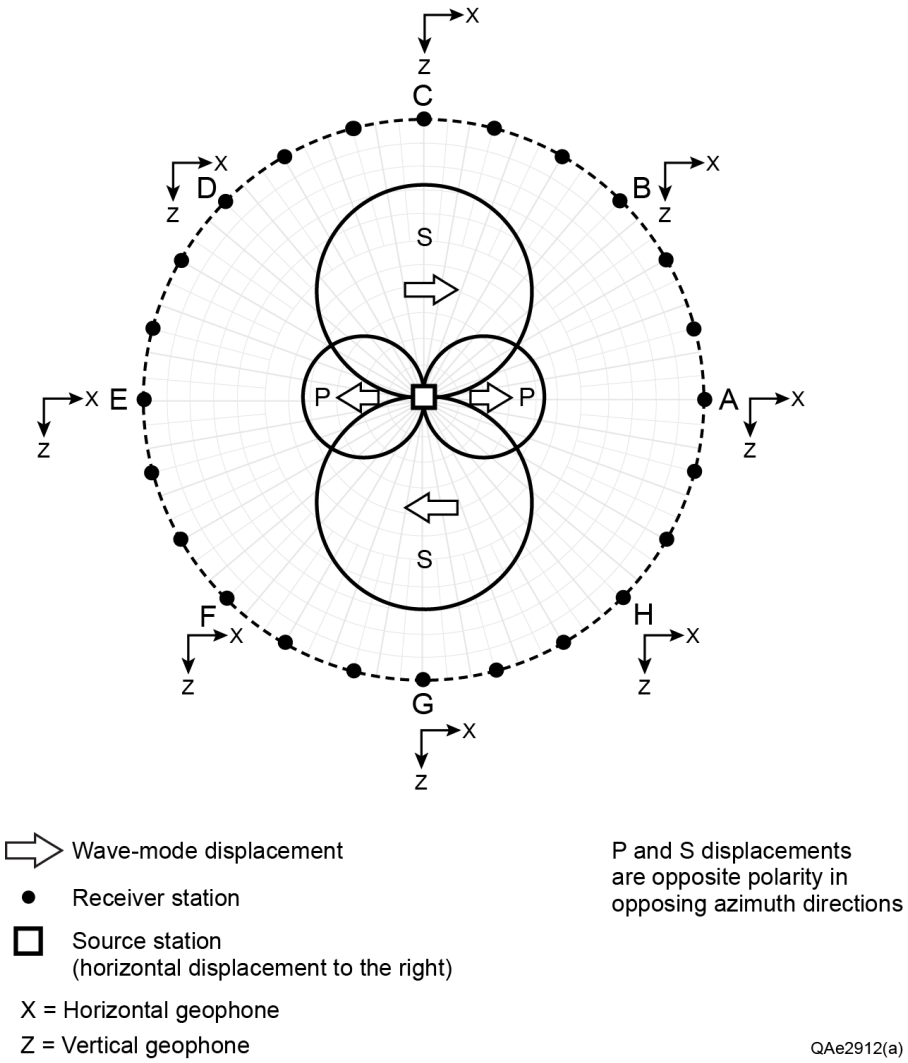


Figure 9. Polarities of P and S displacements created by a horizontal-displacement source when surrounding receivers are deployed as shown.

shown at travel time intervals of 200 ms in Figure 10. The positions of propagating direct-P and direct-S wavefields produced by a horizontal-displacement source are shown for the same travel time intervals in Figure 11. These calculations illustrate the opposite-polarity behavior of the recorded direct-P and direct-S wavefronts that expand away from vertical-displacement-source and horizontal-displacement-source stations in take-off angle directions that differ by $180^{o}$. These opposing data polarities are determined by whether a receiver and the wavefront displacement vector are oriented in the same direction (positive polarity) or in opposite directions (negative polarity). In Figures 10 and 11, wavefront amplitudes are shown as true-amplitude wavelets to better illustrate P and S radiation-strength behavior at all take-off angles.

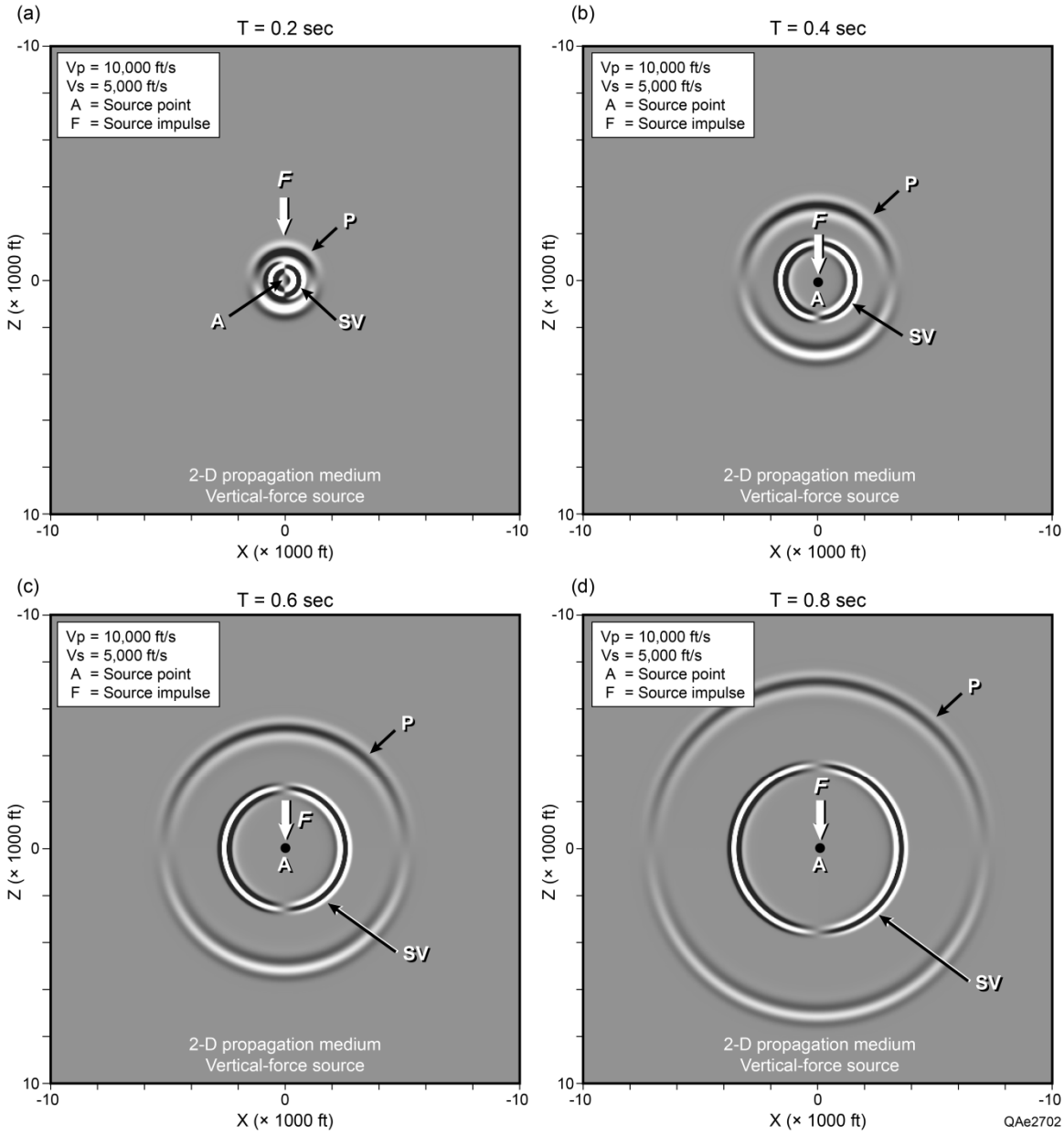


Figure 10. P and S wavefronts propagating away from a vertical-displacement-source station. Note the azimuth-dependent polarity of the wavefronts recorded by the receiver orientations defined in Figures 3a and 3d.

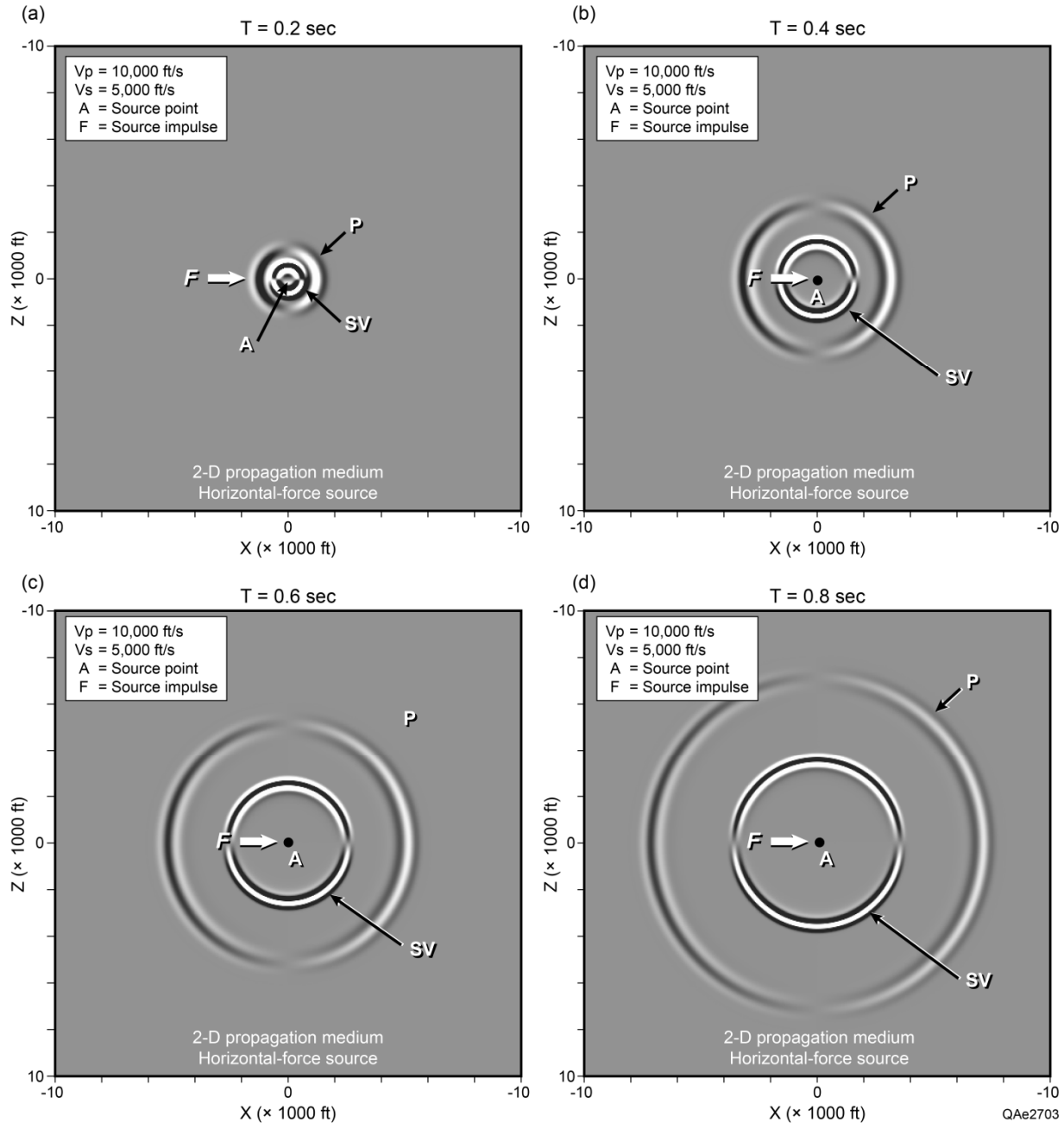


Figure 11. P and S wavefronts propagating away from a horizontal-displacement-source station. Note the azimuth-dependent polarity of the wavefronts recorded by the receiver orientations defined in Figure 4a and 4d.

## P and S Reflection Wavefields

The preceding sections of this report illustrate the physics of the illuminating direct-P and direct-S wavefields that propagate in a medium that has no interfaces. In this section, we insert an interface in the medium and illustrate the nature of the P and S reflection wavefields generated by that interface. For this illustration the earth model displayed as Figure 12 was constructed to create a reflecting interface. The complete propagation space of this model has a constant P-wave velocity ($V_P$ = 10,000 ft/s) and a constant S-wave velocity ($V_S$ = 5,000 ft/s). The reflecting interface is placed 5,000 ft below the source station and involves only a density contrast so that propagation velocity remains constant above and below the interface. The sensor profile is at the same elevation as the source station, 5,000 ft above the reflecting interface. Note that all vertical and horizontal geophones have the same orientation along the receiver line.

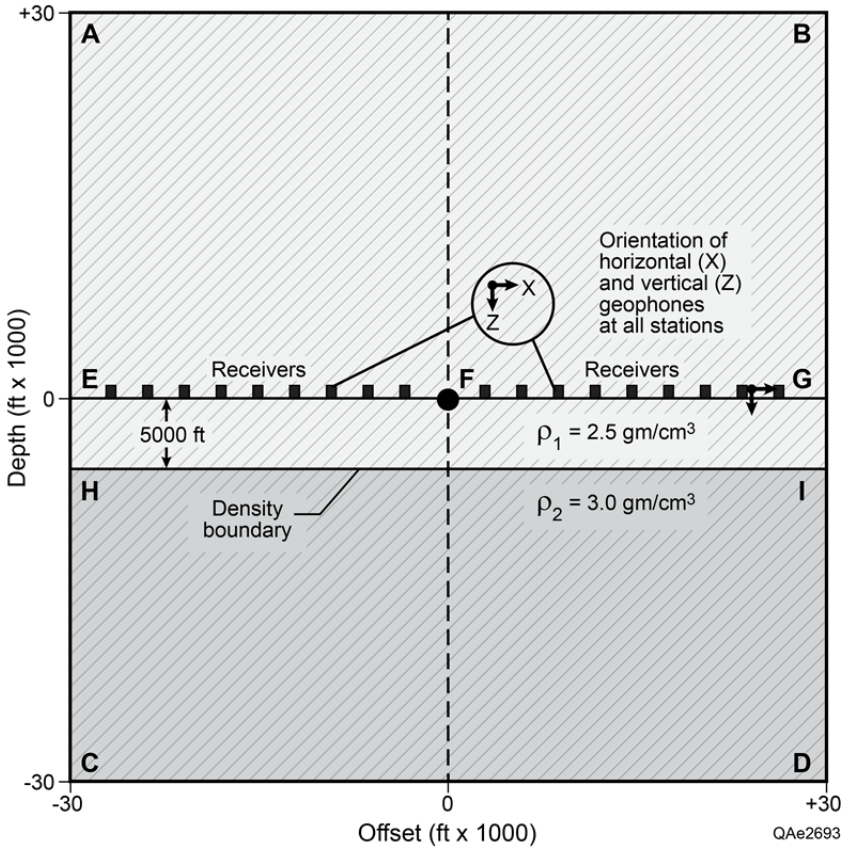


ABCD = Constant velocity earth
Vp = 10,000 ft/s
Vs = 5,000 ft/s

EFG = Receiver profile
F = Source station
HI = Reflection interface (density contrast only)

Figure 12. Constant-velocity earth model with a density contrast interface. Receivers are deployed as a horizontal profile parallel to the reflecting interface.

The reflection wavefields produced by a vertical-displacement source in this model space are illustrated in Figure 13. Reflection wavefields produced by a horizontal-displacement source are displayed in Figure 14. Four data panels are shown in each figure. These same four model outputs will appear in subsequent modeling reports and are described here for future reference.

## P Response

Data generated by the direct-P mode are labeled "*P response*" in Figures 13a and 14a. These data show ALL events that exist because of direct-P propagation in the model space. Some of the events may be recorded by vertical geophones and some may be recorded by horizontal geophones. Every event in a P-response display originates from the direct-P mode produced by the indicated source (vertical-displacement source in Figure 13; horizontal-displacement source in Figure 14). In this report, all reflection events are identified with a hyphenated wave-mode nomenclature. In this notation, the first term of the hyphenated name refers to the downgoing illuminating wavefield, and the second term refers to the reflected wavefield. Note that in Figures 13a and 14a, the first term in the hyphenated reflection-mode nomenclature is "P", indicating the downgoing P mode produced by the source that generated each reflection event. In this discussion, a direct-P mode is the mode generated by calculating the divergence of the P-wave potential function ($\nabla\varnothing$) in equations 1 and 2 of Figure 1.

## SV Response

Data generated by the direct-S mode are labeled "SV *response*" in Figures 13b and 14b. These data show ALL events that exist because of direct-S propagation in the model space. Some of the events may be recorded by vertical geophones and some may be recorded by horizontal geophones. Because every event in Figures 13b and 14b originates from the direct-S mode created by the source positioned at station F, the first term in the hyphenated reflection-event nomenclature attached to each event is "SV". In this discussion, a direct-SV mode is the mode generated by calculating the curl of the S-wave potential function ($\nabla X\psi$) in equations 1 and 3 of Figure 1.

## Vertical Geophone

Data recorded by vertical geophones are labeled "*Vertical geophone*" in Figures 13c and 14c. These data show ALL events that are recorded by vertical geophones. Some of the events may be generated by the downgoing direct-P wavefield, and some may be generated by the downgoing direct-SV wavefield because vertical geophones record vertical displacements $u_z$ produced by the total wavefield ($\nabla\varnothing + \nabla X\psi$). Events appearing in vertical-geophone responses have either P or SV as the first term of the hyphenated reflection-event nomenclature because both direct-P and direct-SV wavefields contribute to vertical-geophone data.

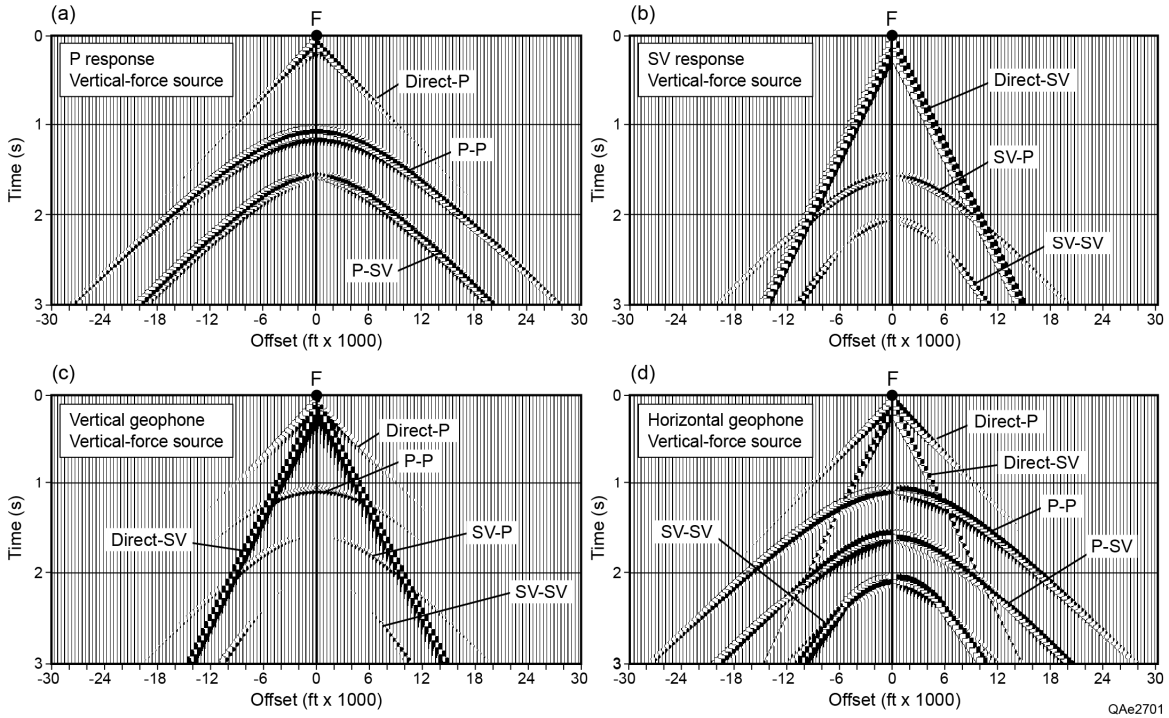


Figure 13. Reflected wavefields resulting from direct-P and direct-S wavefields produced by a vertical-displacement source propagating in the earth model shown as Figure 12.

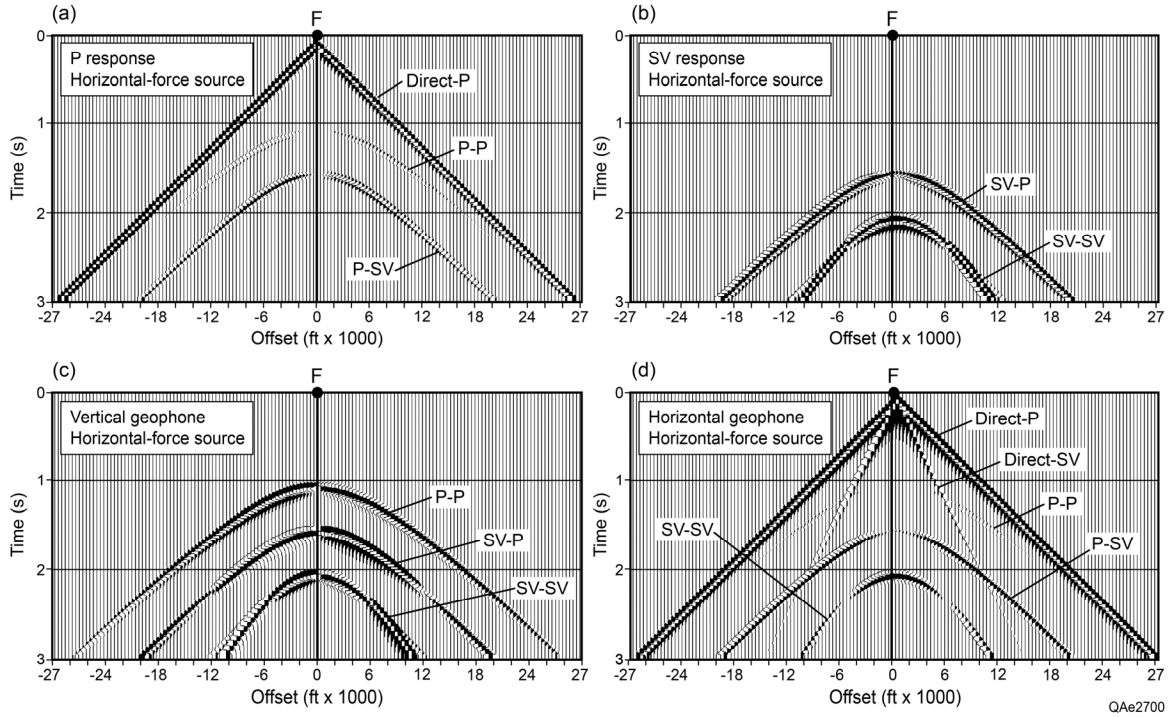


Figure 14. Reflected wavefields resulting from direct-P and direct-S wavefields produced by a horizontal-displacement source propagating in the earth model displayed as Figure 12.

## Horizontal Geophone

Data recorded by horizontal geophones are labeled "*Horizontal geophone*" in Figures 13d and 14d. These data show ALL events that are recorded by horizontal geophones. Some of the events may be generated by the downgoing direct-P wavefield, and some may be generated by the downgoing direct-SV wavefield because horizontal geophones record horizontal displacements $u_x$ produced by the total wavefield $(\nabla\varnothing + \nabla X\psi)$. Events appearing in horizontal-geophone responses have either P or SV as the first term of the hyphenated reflection-event nomenclature because both direct-P and direct-SV modes contribute to horizontal-geophone data.

Several features of the wavefields in Figures 13 and 14 are the effects of the geometrical shapes of the P and S radiation patterns shown in Figures 7b and 7c. For example, the direct-P wave that travels down the horizontal receiver line in Figures 13a, 13c, and 13d is weak because of the null in the P radiation pattern produced by a vertical-displacement source (line AE in Figure 5c). In contrast, the horizontally traveling direct-P wave in Figures 14a and 14d is high amplitude because of the orientation of the P radiation pattern produced by a horizontal-displacement source (line AE in Figure 6c). Similarly, the direct-SV wave in Figures 13b and 13c is robust because a vertical-force source causes SV energy to expand in a horizontal direction (line AE in Figure 5c), but the direct-SV wave in Figure 14d is weak because a horizontal-displacement source creates a null in the SV radiation patterns that expand in a horizontal direction (line AE in Figure 6c).

An important wave physics behavior exhibited by these model data is the opposite-polarity behavior of opposite-offset data when a source displacement vector and a recording sensor are orthogonal to each other, versus the constant-polarity nature of opposite-offset data when a source displacement vector and a recording sensor are oriented in the same direction. In other words, data generated by a vertical-displacement source and recorded by horizontal sensors have opposite polarity in opposite-azimuth directions (arrivals P-P and P-SV in Figure 13d), but data generated by a vertical-displacement source and recorded by vertical sensor do not (Fig. 13c). Similarly, data generated by a horizontal-displacement source and recorded by vertical sensors have opposite polarity in opposite-azimuth directions (P-P arrival in Figure 14c), but data generated by a horizontal-displacement source and recorded by horizontal sensors do not (SV-SV arrival in Figure 14d). Additional examples are:

a) In Figure 13c the P-P reflection has constant polarity for positive and negative offset directions (vertical-displacement source and vertical geophones), but in Figure 13d the P-P reflection has opposite polarity in positive and negative directions (vertical-displacement source and horizontal geophones), and
b) In Figure 14d the SV-SV reflection has constant polarity for positive and negative offset directions (horizontal-displacement source and horizontal geophones), but in Figure 14c the SV-SV reflection has opposite polarity in positive and negative directions (horizontal-displacement source and vertical geophones).

Some aspects of these model results are not realistic representations of real-earth data behavior because of the constant-velocity conditions assigned to the entire model space. Specifically, the SV-SV reflections that are recorded by the vertical geophones in Figures 13c and 14c and the P-P reflections recorded by the horizontal geophones in Figures 13d and 14d would rarely appear, or be as robust, in real-earth data. Low-velocity, near-surface layers would bend P and S raypaths to a near-vertical approach direction at each receiver station and cause P displacements to activate only vertical geophones and SV displacements to activate only horizontal geophones. In this model calculation, reflected P and SV displacements activate both vertical and horizontal geophones because propagation velocities are 10,000 ft/s ($V_P$) and 5,000 ft/s ($V_S$) immediately around all receiver stations, which are the same propagation velocities that exist throughout the model space. Thus no raypath bending occurs near receiver stations in this model. This departure from real-earth reflectivity behavior does not detract from the value of the model results and can be overcome by placing a low-velocity layer immediately below all receiver stations if desired.

## Conclusions

The seismic modeling code now used at EGL is a valuable tool for planning direct-S seismic data-acquisition programs, implementing direct-S and direct-P data-processing strategies, and interpreting direct-P and direct-S data. The code clarifies the basic physics of direct-S and direct-P illumination of targets by vertical-displacement and horizontal-displacement sources. It is particularly valuable to use the code to show the geometrical shapes of direct-P and direct-S radiation patterns, the strengths of P and S illuminating wavefields at various take-off angles from a source station, and the polarities of direct-P and direct-S reflections at positive-offset and negative-offset receiver stations. An important aspect of the code is that it allows reflections to be segregated into four key subsets: (1) all events produced by the downgoing direct-P mode, (2) all events created by the downgoing direct-S mode, (3) all events recorded by only vertical geophones, and (4) all events recorded by only horizontal geophones. The use of this modeling code will improve data-acquisition and data-processing procedures to capture direct-S modes generated by vertical-displacement sources.

## References

Wapenaar, C., P. Herrmann, D. Verschuur, and A. Berkhout, 1990, Decomposition of multicomponent seismic data into primary P and S responses: Geophy. Prosp., v. 38, p. 633-661.